

Quantifying primary oxidation products in the OH-initiated reaction of benzyl alcohol

Reina S. Buenconsejo¹, Sophia M. Charan¹, John H. Seinfeld¹, and Paul O. Wennberg¹

¹California Institute of Technology, Pasadena, CA 91125

Correspondence: Paul O. Wennberg (wennberg@caltech.edu)

Abstract. Benzyl alcohol is a compound found in many volatile chemical products (VCPs), and is widely used in including a number of personal care products and as an industrial solvent. While past work has empirically identified oxidation products, we do not understand explicit branching ratios for first-generation benzyl alcohol oxidation products, particularly over a range of NO_x conditions. We report here the products of the gas-phase oxidation of benzyl alcohol by OH and its dependence on nitric oxide (NO) levels. Using gas chromatography (GC) in tandem with chemical ionization mass spectrometry (CIMS) and gas chromatography with a flame ionization detector (GC-FID), we measure the branching ratios of major fractions to the major gas-phase oxidation products, namely hydroxybenzyl alcohol (HBA) and benzaldehyde. Later-generation oxidation products from both HBA and benzaldehyde pathways are also observed. We find the In particular, catechol is a major gas-phase product of HBA. The fraction of H-abstraction route from benzyl alcohol leading to benzaldehyde formation is unaffected by [NO], with a branching ratio of ~19%. The OH addition route, however, which leads an average branching fraction of (21 ± 10)%. The fraction of OH addition leading to HBA formation, does (36 ± 18)% also does not appear to vary with [NO]. At higher NO, we report a branching ratio for HBA of ~45–47% and as high as ~69% at low NO. We also Consistent with the known high SOA yields of catechol, we find that HBA has a very high secondary organic aerosol (SOA) yield and, therefore, likely contributes to the high SOA yield of benzyl alcohol which under some conditions can approach. Thus, benzyl alcohol and its oxidation products efficiently produce secondary organic aerosol—under some conditions approaching unity. Insights from the present study can help elucidate the chemistry of other atmospherically-relevant aromatic compounds, especially those found in VCPs.

1 Introduction

Recent work indicates the growing importance of volatile chemical products (VCPs) have been recently identified as critical in driving air pollution chemistry, particularly as regulations decline drive a decrease in the contribution of vehicular-based emissions (McDonald et al., 2018; Coggon et al., 2021). VCPs play an important role in air quality because of their high potential to form secondary organic aerosol (SOA); an analysis of VCPs in the Los Angeles Air Basin indicates that VCPs could contribute up to 70% of SOA formation in the Los Angeles Air Basin despite accounting for only approximately 4% of total petrochemical product use (McDonald et al., 2018). Regional scale modeling that includes The inclusion of VCP emission inventories also shows improved agreement with ambient data compared to past models that historically has improved

the agreement of regional scale modeling compared to previous models that did not consider VCP emissions (Seltzer et al., 2021; Pennington et al., 2021). However, because many of the chemicals comprising VCP emissions have not been studied in laboratory settings, their contribution to SOA formation is uncertain. Therefore, additional experimental work on VCPs is still needed.

30 Here, we evaluate the photochemistry of benzyl alcohol, a compound found prominently in VCPs. Benzyl alcohol is used in soaps and perfumes, and is also used as a solvent in the manufacture of paints, inks, lacquers, and epoxies (Wang, 2015). In a previous study, the aerosol mass yield of benzyl alcohol was found to have a high mass yield under a variety of ~~conditions—even conditions—even~~ approaching unity (Charan et al., 2020; Jaoui et al., 2023).

35 Experimental studies, including kinetic experiments on benzyl alcohol, have ~~identified determined that~~ the primary atmospheric oxidative pathway of benzyl alcohol ~~to proceed proceeds~~ via reaction with the OH radical (Bernard et al., 2013; Harrison and Wells, 2009). Harrison et al. calculated that benzyl alcohol reacts with OH at a rate of $(28 \pm 7) \times 10^{-12} \text{ cm}^3 \text{ molecule}^{-1} \text{ s}^{-1}$. The reaction rate with O_3 is too slow to ~~contribute to its oxidation significantly affect to benzyl alcohol mixing ratios~~ in most environments (Harrison and Wells, 2009).

40 Previous experimental studies of benzyl alcohol identified several oxidation products including hydroxybenzyl alcohol (HBA) and benzaldehyde (Burkholder et al., 2017; Harrison and Wells, 2009; Bernard et al., 2013). A theoretical study on the mechanism of benzyl alcohol oxidation initiated by ~~the~~ hydroxyl radicals (OH) also predicted the major oxidation pathways ~~to~~ form benzaldehyde, *i*-hydroxybenzyl alcohol, and *o*-hydroxybenzyl alcohol (Wang, 2015). Other products observed in past experimental studies include ring-opening products, such as but-2-enal and 6-hydroxy-5-oxohex-2-enal (Harrison and Wells, 2009), as well as C6 compounds ~~such as dihydroxy benzene~~ (Bernard et al., 2013). These past experiments were 45 conducted under high NO conditions. Yet, understanding chemical mechanisms and ~~yields branching fractions~~ as a function of NO is important for understanding ~~the impact of its oxidation on~~ urban air quality as NO_x to VOC ratios have been shown to affect OH oxidation of VOCs and as NO_x regimes continue to change in urban settings (Seinfeld and Pandis, 2016; Parker et al., 2020). This is particularly relevant as NO_x continues to decline in many U.S. urban areas (Parker et al., 2020).

50 In this study, we draw on past work which suggests HBA forms via addition of OH to the benzyl alcohol aromatic ring. We experimentally confirm products identified in past work, including products predicted in a theoretical study (Wang, 2015). We also ~~report quantitative values for quantify the branching to~~ HBA, benzaldehyde, phenol, and ~~hydroxy oxopentenal~~⁵-hydroxy-4-oxo-2-pentenal. We find the branching ~~ratios fraction~~ for HBA, the primary oxidation product, ~~depend on NO and range from ~45–69%.~~ Benzaldehyde, the other main oxidation product, is $\sim 36\%$. Benzaldehyde has a branching ~~ratio of ~19% fraction of ~21%~~ ratio of $\sim 19\%$ fraction of $\sim 21\%$.

2 Methods

55 Chamber experiments were conducted to elucidate the chemical mechanism of benzyl alcohol oxidation via OH. First-generation oxidation products were ~~also~~ used to identify important pathways to SOA formation. Two set-ups were used to investigate ~~this chemistry~~: 1.) Gas-phase ~~yields experiments to determine the branching fractions~~ and gas-phase oxidation chemistry; and 2.)

The chemical pathways responsible for SOA formation particle-phase experiments to measure the SOA yields of the primary benzyl alcohol oxidation products.

60 **2.1 Experimental Design**

Gas-phase experiments were conducted in a $\sim 0.8 \text{ m}^3$ FEP Teflon-walled environmental chamber, henceforth referred to as Chamber G. The chamber Chamber G was filled and evacuated multiple times with purified air prior to experiments. Particle-phase experiments were conducted in a 19 m^3 FEP Teflon-walled environmental chamber (henceforth referred to as Chamber P) which was continuously flushed for $> 24 \text{ h}$ prior to experiments. All experiments were run at room temperature ($\sim 22^\circ\text{C}$), 65 low relative humidity ($< 10\% \text{ RH}$), and ambient pressure ($\sim 1 \text{ atm}$). Benzyl alcohol (Sigma Millipore, ReagentPlus $\geq 99\%$) and benzaldehyde (Sigma Millipore, ReagentPlus $\geq 99\%$) were injected into the chamber by flowing warm air over ~~over~~ a measured amount of precursor deposited on a Pall Teflon filter. For gas-phase experiments, ~~2-hydroxybenzyl o-hydroxybenzyl~~ alcohol (HBA) (Sigma Millipore 99%) was injected similarly. Because HBA is a relatively low-volatility compound, in order to achieve sufficiently high concentrations in Chamber P for particle-phase experiments, HBA was dissolved in milliQ water 70 and injected by bubbling purified air through the solution.

For ~~the~~ high NO gas-phase experiments (G1—G2 ~~and~~ G4), methyl nitrite was used as the oxidant precursor. ~~Methyl nitrite was added to the reactor~~ by measuring the pressure of methyl nitrite into an evacuated round-bottom bulb and back-filling the remainder of the bulb volume with nitrogen. NO ($1993 \pm 20 \text{ ppm NO in N}_2$, Matheson) was prepared in a similar manner. For high NO, particle-phase experiments, NO ($506.9 \pm 10 \text{ ppm NO in N}_2$) was injected using a mass-flow controller (Sierra 75 Instruments).

In experiments ~~G1, G3 and G5, P1, and P2~~, hydrogen peroxide (H_2O_2) (Sigma Millipore, 50 wt% in H_2O stabilized) was used as the OH precursor by injecting a known mass ~~(G1, G3, and G5) or volumen (P1 and P2)~~ into a glass bulb and flowing purified air over the liquid droplets ~~to add to the reactor~~. In particle-phase experiments, the H_2O_2 was heated in a water bath ($\sim 42^\circ\text{C}$) during injection.

80 All particle-phase experiments were seeded using a sonicated solution of 0.06 M ammonium sulfate ($(\text{NH}_4)_2\text{SO}_4$). During injection, the seed solution was run through a soft x-ray charge conditioner (TSI Model ~~20883088~~). In all experiments, $\sim 1 \text{ h}$ was allowed after all injections were completed and before the lights were turned on to allow for mixing and collection of adequate background data. In particle-phase experiments, this time was also used to confirm previously calculated chamber wall loss parameters (Charan et al., 2018).

85 Ultraviolet (UV) broadband lights centered around $\sim 350 \text{ nm}$ were used as the light source for photooxidation (Light Sources, Inc.); oxidation duration was determined so that $\sim 10\%$ of the precursor was reacted in gas-phase reactions. The j_{NO_2} and $j_{\text{CH}_3\text{ONO}}$ for Chamber G are $4.4 \times 10^{-3} \text{ s}^{-1}$ and $1.1 \times 10^{-3} \text{ s}^{-1}$, respectively. The j_{NO_2} and $j_{\text{H}_2\text{O}_2}$ of Chamber P are measured to be $4.4 \times 10^{-3} \text{ s}^{-1}$ and $3.2 \times 10^{-6} \text{ s}^{-1}$, respectively, using methods described elsewhere (Zafonte et al., 1977). Additional information about the oxidants is found in Appendix A. Photooxidation was carried out for particle-phase experiments for 90 $> 6 \text{ hrsh}$. This oxidation time corresponds to $\sim 50\text{--}100\%$ ~~about 50–100%~~ reaction of the initial VOC and is congruent with reaction times in the benzyl alcohol studies in (Charan et al., 2020). A summary of experiments can be found in Table 1.

Table 1. Experimental Summary.

height Expt. #	VOC	VOC Concentration [VOC] (ppb)	[NO] (ppb)	Oxidant	[Oxidant] (ppb)	Notes
Gas-phase experiments						
G1	Benzyl Alcohol alcohol	46-539	500-1,000	CH ₃ ONO (300) H ₂ O ₂	2,000	
G2	Benzyl alcohol	60-46	44-500	CH ₃ ONO (370)	300	
G3	Benzyl alcohol	32-523	0-50	H ₂ O ₂ ↗	2,000 ↗	
G4	Benzyl alcohol	60	44	CH ₃ ONO	370	
G4-G5	o-Hydroxybenzyl Benzyl alcohol	538	na-0	na-H ₂ O ₂	2,000	
Particle-phase experiments						
P1	Hydroxybenzyl alcohol	191-12	80-160	H ₂ O ₂ ↗	2,000 ↗	
P2	Benzaldehyde	190-82	14-71	H ₂ O ₂ ↗	2,000 ↗	



2.2 Instrumentation

In the particle-phase experiments, NO and NO₂ were monitored using a commercially available Teledyne T200 NO_x monitor. Temperature and RH were measured by a Vaisala HMM211 probe. In gas-phase experiments, NO_x was monitored using 95 commercially available Teledyne ~~NO_x M200 EU~~M200EU NO_x monitor. Additional instrumentation used ~~used~~ in gas-phase and particle-phase experiments is described in the following sections.

2.2.1 Particle Mass Detection

Particle size distribution was monitored using a custom-built scanning mobility particle sizer (SMPS) which uses a commercially available ~~308100 TSI Differential Mobility Analyzer~~TSI 3081 differential mobility analyzer (DMA) and a TSI 100 3010 condensation particle counter (CPC) (Mai, 2018). Prior to the DMA inlet, a soft x-ray charger provided a known charge-distribution. Wall loss corrections and subsequent SOA yields were calculated based on ~~extensive~~ work and model development explained in Charan et al. (2018) and Huang et al. (2018), and detailed more specifically for these experiments in ~~Charan et al.~~ Charan et al. (2020). SOA yields were calculated based on a ratio of the mass of the VOC precursor reacted and the formation of SOA~~mass of the SOA formed~~:

$$105 \quad Y = \frac{\Delta SOA}{\Delta VOC \text{ precursor}} \quad (1)$$

Here, ΔSOA is the change in the aerosol mass concentration while accounting for any aerosol loss to the chamber walls. Aerosol density was assumed to be 1.04 g cm⁻³ based on past work on benzyl alcohol (Charan et al., 2020; Li and Cocker, 2018).

2.2.2 Gas-Phase Detection

110 A chemical ionization triple quadrupole mass spectrometer (CIMS) with a CF₃O⁻ reagent ion was used to monitor gas-phase compounds in particle-phase experiments. This set up has been described in detail elsewhere (Schwantes et al., 2017). In brief, the CIMS operates by reacting with the gas-phase compounds in the sample that have an electron affinity sufficient to bind with the reagent ion cluster (CF₃O⁻). Sampled compounds that are acidic may also transfer a ~~fluoride~~fluoride ion (F⁻). The sample is then detected by a Varian 1200 triple quadrupole mass analyzer which measures masses from m/z = 50 to 330. A 115 custom-built inlet to the CIMS was set at a constant temperature, 25°C.

Benzaldehyde, one of the primary products of benzyl alcohol OH oxidation, is not detectable using the CF₃O⁻ CIMS. Thus an HP 6890N gas chromatograph with a flame ionization detector (GC-FID) was used in ~~experiments in Chamber P~~experiments G1, G3, G5, P1, and P2 to detect benzaldehyde. Experiments were run with a DB5 column. Information on the temperature profile and GC operation can be found in Appendix C.

120 In gas-phase experiments in Chamber G, the GC-CIMS was used to monitor the gas phase precursors and subsequent photooxidation products. This experimental setup is described in detail elsewhere (Vasquez et al., 2018; Xu et al., 2020) Here, the GC-CIMS was operated in ~~both~~ negative mode using CF_3O^- , ~~and for experiments G2 and G4,~~ in positive mode using NO^+ . The chemistry involving CF_3O^- is ~~the same as that~~ described previously and detailed in Appendix B (Vasquez et al., 2018; Crounse et al., 2006). In positive mode, NO^+ complexes with less acidic compounds and can be detected at $[\text{M}+\text{NO}^+]$ (also described further in 125 Appendix B). A 2 m Restek RTX-1701 column was used for all experiments for better chromatographic resolution of certain isomers. GC samples were cryogenically trapped at -20°C on the column. Additional information on the GC-CIMS operation is in Appendix C.

2.2.3 Calibrations

~~Sensitivities of analytes to instrumentation was generally determined~~ The sensitivities for analytes in the GC-CIMS were 130 generally determined from prepared standards and quantified using Fourier transform infrared (FTIR) spectroscopy. The GC-FID and the CIMS in experiments P1 - P2 were calibrated by injecting the analyte of interest into a ~100L Teflon pillow bag using the same injection method as described ~~previously~~ for Chamber G. The sample was then measured via a FTIR spectrometer with a pathlength of 19 cm. ~~The reference Reference~~ FTIR spectra from the Pacific Northwest National Laboratory (PNNL) database were used to tabulate cross sections ~~to and~~ determine exact concentrations ~~Schwantes et al. (2017)~~ 135 (Schwantes et al., 2017). The pillow bag was then diluted using dry N_2 and sampled to determine the instrumental sensitivity (Xu et al., 2019).

Several ~~of the~~ substrates involved in this study are relatively non-volatile, leading to challenges with quantitative transfer into and out of the FTIR cell. Therefore some of the GC-CIMS sensitivities were ~~estimated from the measured sensitivity to proxy compounds and using permeation tubes~~ determined using calculated polarizabilities and dipole moments to determine 140 the ion-molecule collision rates of the analytes with the reagent ion relative to the collision rates with reference calibrants (??). Additional information on this procedure can be found in ~~SI.2. In short, permeation tubes with the known amounts of the calibrants were connected to the instrument to correlate substrate quantity (weight) and instrument signal~~. Appendix B.

2.3 Secondary Chemistry

2.3 Corrections

145 2.3.1 Vapor-wall Loss

Vapor wall loss was examined by sampling benzyl alcohol (and products) prior to oxidation and post-oxidation. Vapor wall loss periods were as long as or on timescales with similar orders of magnitude to the oxidation periods. During these sample periods, the signal of oxidation products remains stable. Thus, no vapor-wall loss correction is applied. This is congruent with past work on quantifying benzyl alcohol products, as well as other work quantifying first-generation gas-phase products, which typically

150 considered gas-phase wall loss to be negligible (Charan et al., 2020; Jaoui et al., 2023; Bernard et al., 2013; Harrison and Wells, 2009)

~

2.3.2 Secondary Chemistry

Oxidation products of benzyl alcohol react as they are formed. ~~These~~ for some of the oxidation products, their rate coefficient for reaction with OH is faster than benzyl alcohol. ~~These secondary~~ losses were accounted for when calculating branching ratios in estimating the branching fractions of benzyl alcohol products. ~~Branching ratios (BR~~ which are reported in Table 4. Branching fractions (BF) were calculated as:

$$\text{BR BF} = Y \times CF \quad (2)$$

The gas-phase ~~yield, Y~~, ~~time-dependent yield (Y)~~ is calculated as the amount of oxidation product formed divided by the amount of precursor reacted. To solve for the correction factor, ~~CF(CF)~~, a constant [OH] is assumed for the time-dependent product concentration, which can be described as:

$$[\text{Product}]_t = [\text{BA}]_0 \times \frac{Y \times k_{\text{BA}}}{k_{\text{BA}} - k_{\text{Product}}} \times [e^{-k_{\text{Product}}[\text{OH}]t} - e^{-k_{\text{BA}}[\text{OH}]t}] \quad (3)$$

The time-dependent concentration of benzyl alcohol is described as:

$$[\text{BA}]_t = [\text{BA}]_0 \times e^{-k_{\text{BA}}[\text{OH}]t} \quad (4)$$

Therefore ~~CF, the correction factor, CF~~ is defined as:

$$165 \quad CF = \frac{k_{\text{BA}} - k_{\text{product}}}{k_{\text{BA}}} \times \frac{1 - [\text{BA}]_t/[\text{BA}]_0}{([\text{BA}]_t/[\text{BA}]_0)^{k_{\text{product}}/k_{\text{BA}}} - ([\text{BA}]_t/[\text{BA}]_0)} \quad (5)$$

~~This correction factor is described elsewhere in greater detail (Atkinson et al., 1982). The kinetic rate constants used to solve for Eq. 5 can be found in Table 2. For HBA, the correction factor ranged from ~4–8%, for phenol < 0.2%, benzaldehyde ~0.6–2%, and hydroxy octenental ~0.6–2.9%. This correction factor is described elsewhere in greater detail (Atkinson et al., 1982). The correction factors are presented in Table 3.~~

170 The time traces for HBA and catechol are consistent with the rapid rate of reaction of HBA with OH, which produces catechol in high yield. This was previously reported by Bernard et al. (2013). Because the kinetics of OH with HBA are unknown, we estimate $k_{\text{OH+HBA}}$ using the kinetic rate constant of catechol (Appendix H).

Table 2. Kinetic rate constants used to determine the correction factors for branching fraction calculations.

Compound	k_{OH} ($\text{cm}^3 \text{molec}^{-1} \text{s}^{-1}$)	Kinetic rate
heightBenzyl alcohol	$(2.8 \pm 0.7) \times 10^{-11}^*$	$(2.8 \pm 0.7) \times 10^{-11}^*$
Benzaldehyde	$(1.29 \pm 0.32) \times 10^{-11}^+$	$(1.29 \pm 0.32) \times 10^{-11}^+$
<i>o</i> -Hydroxybenzyl alcohol	$(4.26 \pm 0.22) \times 10^{-11}^{\ddagger}$	Phenol
Butenedial	$(2.83 \pm 0.57) \times 10^{-11}^{\ddagger\ddagger}$	$(3.45 \pm 0.34) \times 10^{-11}^{**}$
Catechol	$(3.45 \pm 0.34) \times 10^{-11}^{**}$	$(1.04 \pm 0.21) \times 10^{-10}^{***}$
HBA		$(5.59 \pm 2.2) \times 10^{-11}^{\ddagger}$
height		

constants used to determine the correction factors for branching ratio calculations. *Harrison and Wells (2009) and Bernard et al. (2013). †Calvert et al. (2002). ‡US EPA EPI Suite. ‡‡Rinke and Zetzs (1984). ** Martín et al. (2013). Note that for hydroxy oxopentenal, the k_{OH} for butenedial is used to calculate the correction factor.

*Harrison and Wells (2009) and Bernard et al. (2013). † Calvert et al. (2002). ‡‡ Rinke and Zetzs (1984). ** Martín et al. (2013). *** (?). Note that for 5-hydroxy-4-oxo-2-pentenal, the k_{OH} for butenedial is used to calculate the correction factor. ‡Calculated in the present work.

Compound	Correction Factor
HBA	1.4
Benzaldehyde	1.1
5-hydroxy-4-oxo-2-pentenal	1.2
Phenol	1.2

Table 3. Calculated correction factors based on Eq. 5, averaged over all experiments.

3 Results and Discussion

3.1 Gas-Phase Branching Ratiosbranching fractions

175 Gas-phase products were identified in Experiments G1-3 (Table 4 and Figure ??). The oxidation secondary losses of first generation products were minimized by limiting the reaction of benzyl alcohol to $<10\%$ $\sim 10\%$. The oxidation of benzyl alcohol forms C7 products, such as HBA and benzaldehyde. Additionally, we observed small yields of C6 products, (products) such as phenol and subsequent oxidation products such as catechol, as well as ring-opening products such as hydroxy oxopentenal. These and other later-generation oxidation products, including fragmentation products, are reported. (such as 5-hydroxy-4-oxo-2-pentenal).

180 A list of products and their corresponding CIMS chemistry can be found in Appendix D.

Together, these products account for $65 \pm 32\%$ of the loss of benzyl alcohol. The lack of mass closure may reflect the impact of the endo-cyclization route that is known to result in a large diversity of products (Xu et al., 2020) many of which may be unmeasureable with CF_3O^- CIMS or have very low vapor pressure, likely yielding aerosol (see Particle-Phase Results).

NO dependence of yields for hydroxybenzyl alcohol (HBA), benzaldehyde, hydroxy oxopentenal, and phenol.

185 3.1.1 Hydroxybenzyl Alcohol and Benzaldehyde

Table 4. Branching Fraction Results of Gas-Phase Yield Experiments

Experiment	Hydroxybenzyl Alcohol Yield	Benzaldehyde Yield	Hydroxy Oxopentenal Yield	5-hydroxy-4-oxo-2-pentenal	Phenol Yield
1,000 ppb NO	(30 ± 14)%	(22 ± 6.0)%		(4.0 ± 1.6)%	(1.3 ± 0.58)%
500 ppb NO	(45 ± 27)% (40 ± 20)%	(19 ± 12)%		(11 ± 6.8)% (8.8 ± 2.7)%	(0.66 ± 0.42)% (4.2 ± 1.9)%
50 ppb NO	(37 ± 19)%	(21 ± 6.0)%		(8.6 ± 3.0)%	(2.6 ± 1.2)%
44 ppb NO	(47 ± 29)% (39 ± 20)%	(31 ± 20)%		(8.0 ± 4.9)% (5.9 ± 2.3)%	(1.5 ± 0.96)% (1.2 ± 0.58)%
0 ppb NO	(69 ± 44)% (34 ± 17)%	(19 ± 12)% (14 ± 4.0)%		(7.3 ± 4.6)% (3.4 ± 1.4)%	(1.1 ± 0.68)% (1.3 ± 0.58)%
Mean height	(36 ± 18)%	(21 ± 10)%		(5.5 ± 1.9)%	(2.1 ± 0.97)%

We sought to quantify the yield. Here, we quantify the branching fractions of the primary benzyl alcohol oxidation products—HBA and benzaldehyde—under low and high NO conditions. Previous studies of benzyl alcohol oxidation were generally performed under high NO conditions. Thus, we are interested in understanding the extent to which NO affects benzyl alcohol chemistry.

190 While HBA is not currently included in the Master Chemical Mechanism (MCM) scheme (Jenkin et al., 2003; Bloss et al., 2005), its formation is predicted and identified in past work on benzyl alcohol kinetics and mechanisms (Calvert et al., 2002; Bernard et al., 2013; Wang, 2015; Bloss et al., 2005; Jenkin et al., 2003). HBA forms via the addition of the OH radical to the aromatic ring. This leads to a radical intermediate which is stabilized by the electron delocalization of the remaining conjugated system. An additional hydrogen abstraction stabilizes the radical intermediate. Subsequent abstraction of hydrogen by oxygen restores the aromaticity. We calculated the amount of HBA formed from benzyl alcohol oxidation from the gas-phase experiments conducted in Chamber G (Experiments G1–3, G1–G5 in Table 1). We found that the branching ratio of HBA decreases with increasing NO (Figure ??). When we find the branching fraction of HBA to be invariant with [NO] is greater than 44 ppb, we found the HBA branching ratio is ~ (45 ± 27)% – (47 ± 29)% and in the absence of NO, we found the yield is larger, (69 ± 44)%. Masses corresponding to later generation oxidation products of HBA included further OH additions to the aromatic ring, such as dihydroxybenzyl alcohol. By averaging over all experiments and accounting for systematic error, we estimate the averaged branching fraction of HBA to be (36 ± 18)%. The primary oxidation product of HBA appears to be catechol (Appendix H). See Section 3.1.2 for a more detailed discussion of how C6 oxidation compounds are formed. Dihydroxy benzyl alcohol was observed in modest quantities, but given its low vapor pressure we are not able to accurately measure the yield. We also observed masses that corresponded to fragmentation products observed in past studies or believed to form via theoretical calculations such as hydroxyoxopropanal (Harrison and Wells, 2009; Wang, 2015; Jaoui et al., 2023). The mechanism for HBA formation and subsequent chemistry can be found in (See Figure 1). Figure 1. This mechanism is based on observed compounds in the present study as well as our understanding of aromatic systems in general. An additional summary of compounds detected can be found in Appendix D.

195 Benzaldehyde forms via initial hydrogen abstraction from the CH₂OH group followed by addition of O₂ and subsequent loss of HO₂. Benzaldehyde was measured via NO⁺ CIMS in Chamber G experiments G2 and G4 and via GC-FID in experiments G1, G3, and G5. The NO⁺ signal is highly water-dependent and therefore less stable than the CF₃O[−] signal. Therefore, it was difficult to confidently quantify the benzaldehyde yield. We estimated the yield is ~19%. However, the benzaldehyde branching

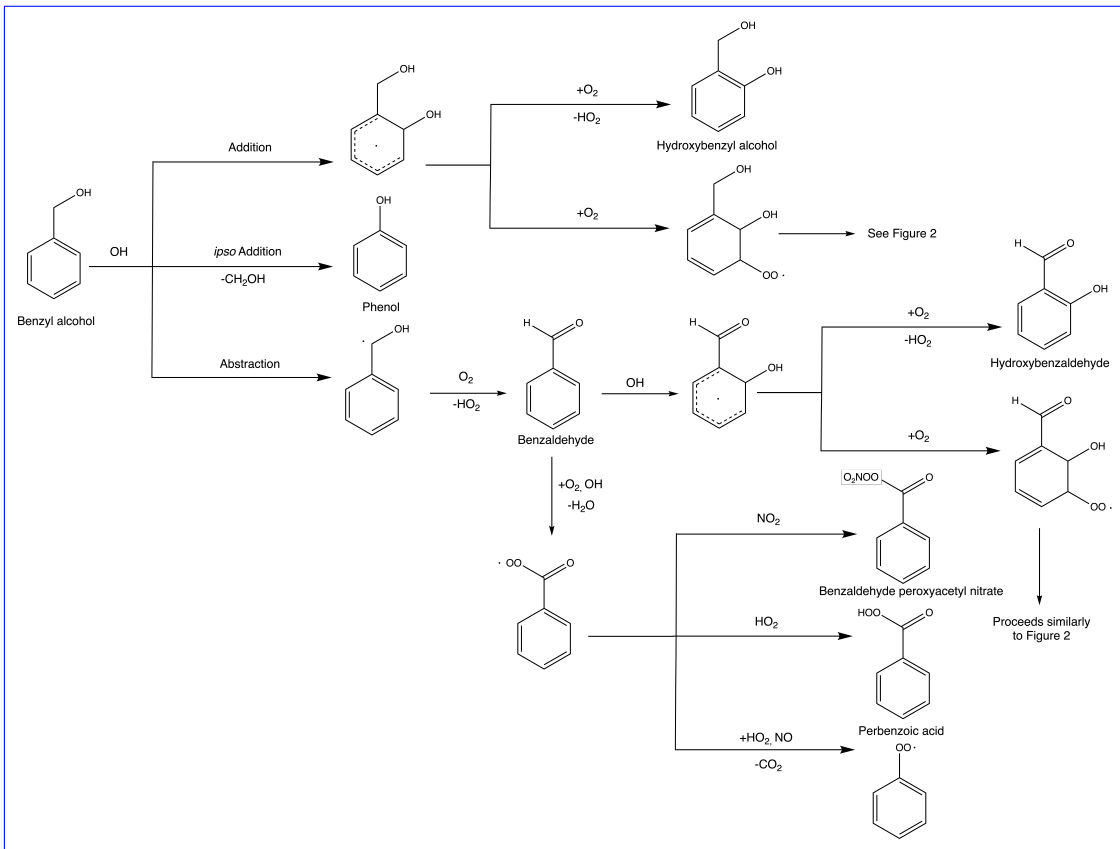


Figure 1. Primary reactive pathways for OH-initiated oxidation of benzyl alcohol.

fraction using the NO^+ and GC-FID are in reasonable agreement. We report an averaged branching fraction of $(21 \pm 10)\%$ under high and low NO conditions, consistent with the expectation that this channel ~~that~~ should not have NO dependence when NO 215 is less than several ppm. ~~Bernard and coauthors quantified the yield of benzaldehyde to be (?)~~. Consistent with our findings, others have quantified the branching fraction to benzaldehyde of 25% ~~Bernard et al. (2013)~~. Since benzaldehyde forms via peroxybenzaldehyde, the intermediate may stabilize to ~~(Bernard et al., 2013)~~. Oxidation of benzaldehyde by OH can go on to form other closed shell products such as ~~hydroperoxide benzaldehyde, and nitrate benzaldehyde~~ benzyl hydroperoxy and benzaldehyde peroxyacetyl nitrate ~~(Calvert et al., 2002)~~. We observe that the oxidation of benzaldehyde by OH also produces ~~hydroxy benzaldehyde following chemistry analogous to the formation of HBA from benzyl alcohol~~. Benzaldehyde can also ~~continue to react via OH addition to the aromatic ring to form products such as hydroxy benzaldehyde~~.

220

3.1.2 C6 Compounds

A previous study of the chemical composition of the SOA formed via OH oxidation of benzyl alcohol observed C6 compounds, such as nitrocatechol (Charan et al., 2020; Jaoui et al., 2023). In the present study, we observed nitrocatechol as

225 well as other C6 compounds such as phenol and catechol. Past work has proposed C6 products can form from ~~benzaldehyde oxidation (Figure ??) (Schwantes et al., 2017; Namysl et al., 2020)~~ the loss of CH_2O from benzaldehyde following OH addition (Schwantes et al., 2017). Further reaction with ~~NO leads to alkoxy benzene which can then stabilize to phenol. Phenol and other O₂ leads to phenol. Other~~ C6 products ~~can also form by~~ ~~may also form via~~ hydrogen abstraction from the ~~CH₂OH group to form a formaldehyde leaving group~~ CH_2O group in benzaldehyde and subsequent loss of CO_2 . Wang (2015) estimated the 230 barrier to decomposition is too high for significant yields of phenol, though predicted low yields of phenol via decomposition of the HBA radical adduct to form phenol and ~~methanol~~ CH_2OH which will react with O_2 to form formaldehyde. However, Wang estimated the barrier to this decomposition was too high for significant formation of phenol. In the present study we observed ~~small initial yields of phenol < 1% initial branching fractions of phenol < 5%~~. We observed that the ~~yield branching fraction~~ of phenol decreases with decreasing NO, consistent with past studies showing the mechanism for phenol formation 235 depends on NO mixing ratio (Xu et al., 2020).

~~Phenol may form via the HBA radical adduct.~~

We observed C6 compounds in both gas-phase and particle-phase experiments. Phenol and other C6 aromatic compounds react rapidly with OH to form other oxygenated aromatic compounds ($\leq 2.7 \times 10^{-11} \text{ cm}^3 \text{molecule}^{-1} \text{s}^{-1}$) (Calvert et al., 2002). Thus, despite relatively low yields of phenol in the first generation of this chemistry, we ~~We~~ observed many C6 products in the 240 aerosol, ~~likely oxidation products of catechol~~. Wang (2015) also predicts a considerable yield of nitroaromatics. In high NO conditions, we observed nitrophenol in gas-phase and particle-phase experiments. Furthermore, in past work, nitrocatechol is identified as an important compound in the chemical composition of aerosol formed from benzyl alcohol oxidation (Charan et al., 2020).

3.1.3 Fragmentation and Ring-Opening Products

245 Notable fragmentation products include hydroxy oxopentenal and butenedial, the latter of which is also reported elsewhere (Harrison and Wells, 2009; Birdsall et al., 2010). We expect a bicyclic peroxy intermediate forms, congruent with the chemistry of other aromatic systems, which leads to, among other products, ring-opening and fragmentation compounds (Calvert et al., 2002). In higher NO conditions, the bicyclic peroxy intermediate goes on to form a bicyclic alkoxy intermediate which eventually 250 fragments to form products such as hydroxy oxopentenal. Thus, as NO increases, the yield of hydroxy oxopentenal also increases. Nonetheless, though, at low NO conditions, fragmentation products still formed in significant quantities possibly because alkoxy formation may occur from the reaction of HO_2 with the precursor RO_2 (Table 4). This behavior is congruent with that of other aromatic systems, such as toluene, in which increased NO favors formation of this ring-opening products, in part due to the formation of a bicyclic peroxy radical (Figure 2) (Birdsall et al., 2010). Notably, in other aromatic systems 255 where the bicyclic intermediate forms, so too can a fragmented epoxide form (Figure 2) (Birdsall et al., 2010). As found in other systems, epoxides can effectively lead to SOA formation (Paulot et al., 2009; Chan et al., 2010). Other fragmentation products found in Jaoui et al. also suggest that fragmentation products can form with high O:C ratios and may quickly partition to SOA (Jaoui et al., 2023).

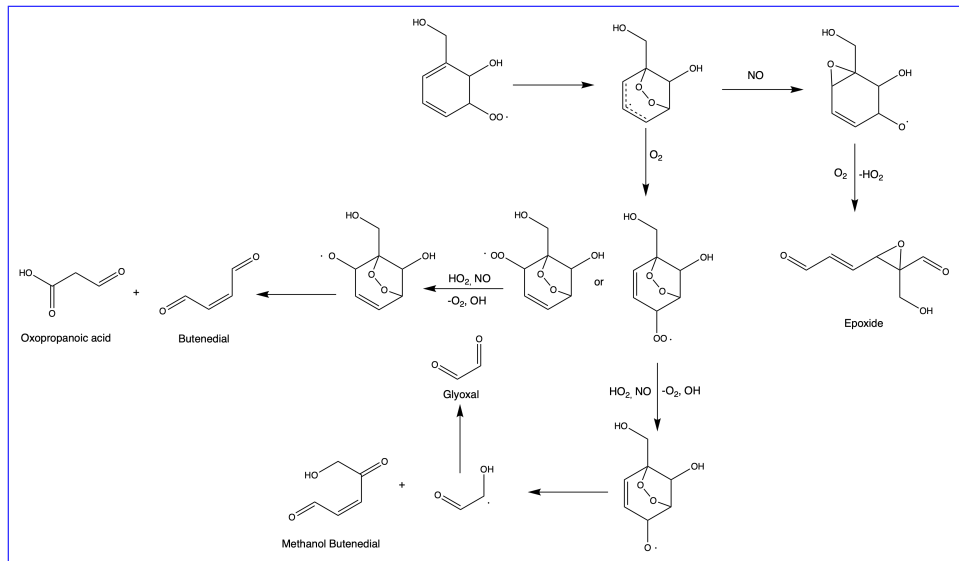


Figure 2. Following addition of OH to the aromatic ring, a bicyclic intermediate can form which can eventually [lead to form fragmentation products](#). Here, we detect products with masses congruent with both the [hydroxy oxopentenal](#) [5-hydroxy-4-oxo-2-pentenal](#) and epoxide products.

3.2 Particle-Phase Results

~~Because HBA has a much lower vapor pressure than benzaldehyde, HBA likely contributed more to SOA formation in benzyl alcohol oxidation than benzaldehyde. This hypothesis was tested by conducting SOA experiments using HBA and benzaldehyde as the VOC precursors (P1–2).~~

260 We estimate the relative contributions of HBA and benzaldehyde to benzyl alcohol SOA formation by conducting individual SOA yield experiments using HBA and benzaldehyde as the VOC precursors. Conditions for SOA experiments were selected to match those of the benzyl alcohol SOA yield experiments in Charan et al. (2020). In brief, experiments were conducted with ~ 80 ppb of initial NO, ~ 80 ppb of VOC precursor, and $\sim 1 \times 10^4$ cm^{-3} of 265 inorganic seed aerosol. SOA yield results were calculated using two treatments: one where the proportionality factor, ω , was set to unity and another in which $\omega=0$. In the $\omega=0$ case, oxidation products with a sufficiently low vapor pressure to condense were assumed to do so only on suspended particles and not on particles that had deposited on the chamber walls (Weitkamp et al., 2007). When $\omega=1$, on the other hand, condensable oxidation products and particles deposited on the chamber walls during the experiment were assumed to be in equilibrium with one another (Weitkamp et al., 2007).

270 Figure 3 shows results for SOA yield experiments using benzaldehyde and HBA. Note the OH exposures for benzaldehyde and HBA in these experiments were $\sim 2.8 \times 10^{10}$ ~~approximately~~ 2.8×10^{10} molecule s cm^{-3} and $\sim 2.8 \times 10^{11}$ 1.4×10^{10} molecule s cm^{-3} , respectively, which corresponds to ~ 26 min to 52 min ~ 8.6 h of OH exposure on a typical Los Angeles summer day (Appendix F) (Griffith et al., 2016). Both experiments were allowed to react for the same amount of time, ~ 400 ~ 350 minutes, to compare to the SOA yield experiments conducted in Charan et al. (2020). Therefore, we report the SOA 275 yields of HBA and benzaldehyde at $t = 400$ mins (SOAY_{400mins}) 350 mins (SOAY_{350mins}), rather than at an equilibrium point. In

At the upper bound, ($\omega = 1$), $\text{SOAY}_{400\text{mins}}$ $\text{SOAY}_{350\text{mins}}$ of HBA is 1.2 ± 0.14 and in $(87 \pm 9)\%$ and at the lower bound ($\omega = 0$), 0.97 ± 0.13 $\text{SOAY}_{350\text{mins}}$ of HBA is $(69 \pm 9)\%$. For benzaldehyde, we report an upper bound of $\text{SOAY}_{400\text{mins}}$ 0.35 ± 0.039 $\text{SOAY}_{350\text{mins}}$ $(67 \pm 17)\%$ and a lower bound of 0.28 ± 0.039 $(46 \pm 17)\%$. While comparing $\text{SOAY}_{400\text{mins}}$ $\text{SOAY}_{350\text{mins}}$ is helpful in determining which pathways (addition versus abstraction) contribute to the high SOA yield of benzyl alcohol, this value 280 does not necessarily inform atmospherically relevant SOA yields of benzaldehyde and HBA as inputs for models because modeled reaction time and conditions may not exactly match experimental ones. Therefore, we report the parameterized fit of the SOA yields as a function of absorbing organic mass concentration (M). In either case, it is clear that the subsequent oxidation of benzaldehyde and HBA contribute significantly to the total SOA yield observed in Charan et al. (2022).

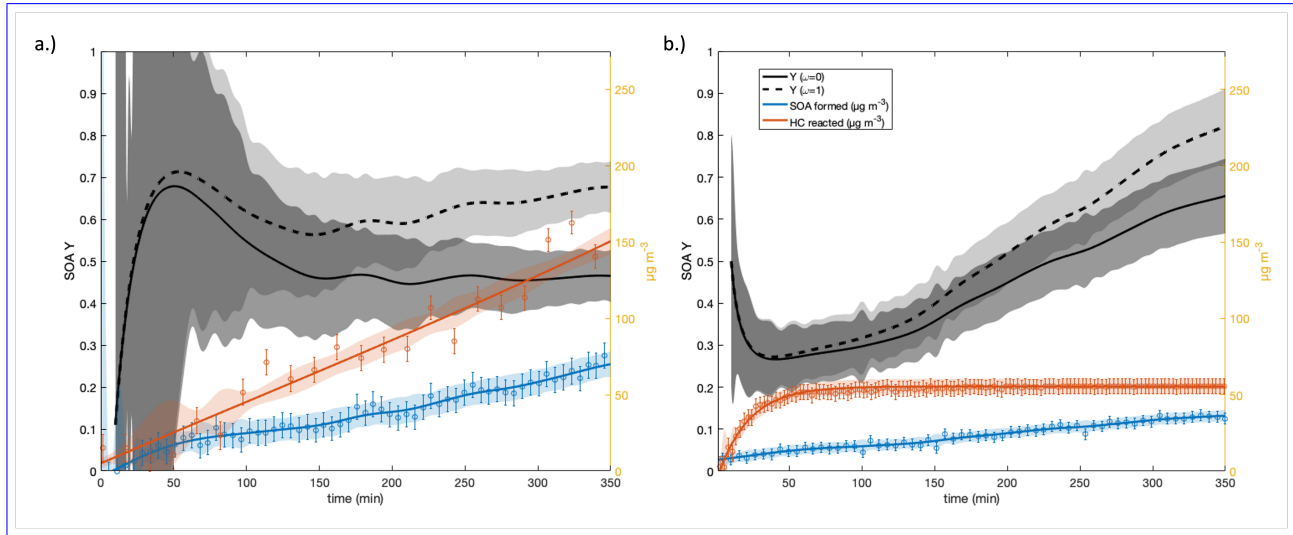


Figure 3. Wall-loss corrected SOA yields of benzaldehyde (a) and HBA (b). Solid yields are calculated assuming ω is zero. Dotted yields are calculated assuming ω equals unity. Red data are the amount of VOC precursor reacted in $\mu\text{g m}^{-3}$. Data displayed in blue are SOA formed in $\mu\text{g m}^{-3}$. Note that the first 10 minutes of SOA yield data are excluded because of the relatively low sensitivity and thus high errors in detecting the amount of hydrocarbon reacted and SOA formed at the start of an experiment.

We follow a one-product parameterization method that follows the multiple paramterization described in Odum et al. 285 parameterization described in Odum et al. (1996) where,

$$Y = M_o \times \left(\frac{\alpha K_{om}}{1 + K_{om} \times M} \right) \sum_i^n \frac{\alpha_i \times K_{om,i}}{1 + K_{om,i} \times M_o} \quad (6)$$

Here α , K_{om} is the partitioning coefficient and where α is a constant relating the total concentration of products formed with the amount of organic gas-phase mass reacted. Two parameters were used to fit the present data. The parameters in Equation 6 were chosen by minimizing the least square fit to the data (Appendix ??). Results for benzaldehyde SOA yield are graphed 290 in Figure 4 ($\alpha = 0.34 \pm 0.013$ and $K_{om} = (9.4 \pm 1.2) \times 10^{-3}$ for $i = 2$, $(\alpha_{i=1} = 0.64$ and $\alpha_{i=2} = 0.64$, $K_{om,i=1} = 0.17$ and $K_{om,i=2} = 1.2$).

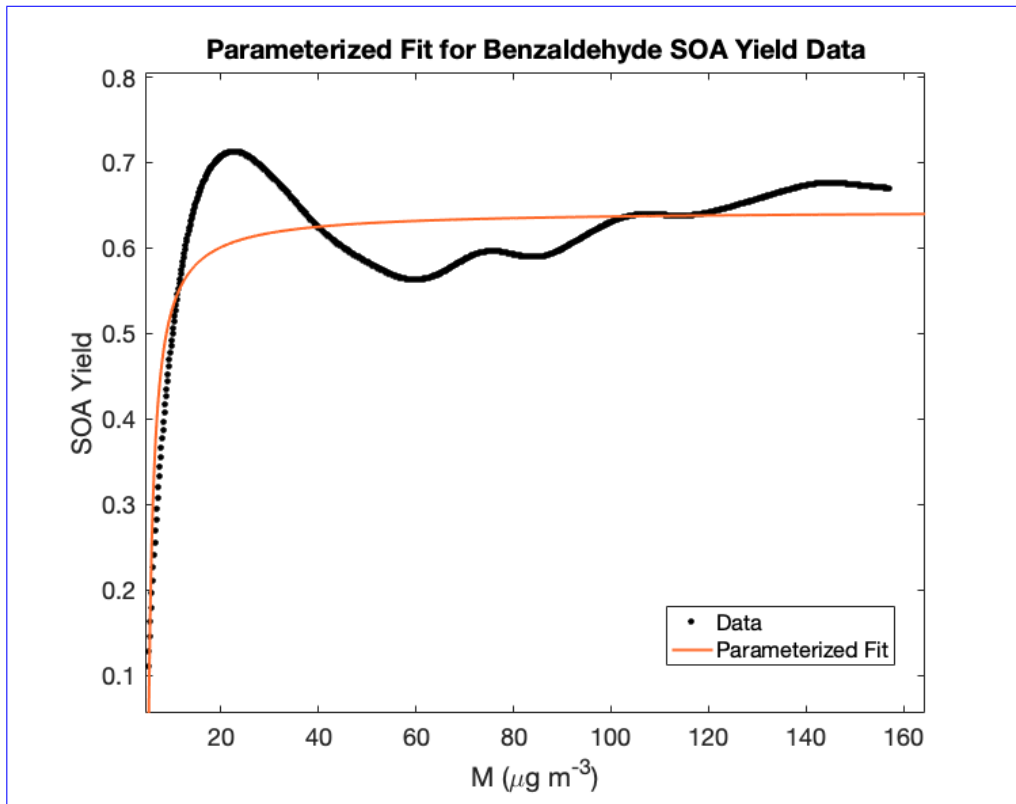


Figure 4. Parameterization of SOA yield data as a function of organic mass reacted. Because SOA yields did not stabilize in these experiments, parameterization can be useful in contextualizing SOA yields under atmospherically relevant conditions.

For HBA, this approach becomes more complicated. The Odum et al. approach uses the steady state approximation (SSA) which states that the derivative of the concentration of an intermediate species appears to be zero. In other words, we assumed an approximately steady state of first-generation oxidation products which are reacting at roughly the same rate as their formation. The rates of reaction of HBA and subsequent oxidation products were likely unequal because the HBA reacts away early in the experiment; therefore, the SSA was not a sufficient approximation and so, we did not use the two-parameter Odum et al. fitting for HBA.

295

300

At $t = 400 = 350$ mins, unreacted benzaldehyde remained in the chamber whereas all of the HBA reacted within the $t < 1\text{ h}$ first hour of the experiment. This may indicate that the SOA formed in the benzaldehyde experiments is from the very rapid chemistry of subsequent generation oxidation products, as is the case with toluene. In the HBA experiments, most of the SOA is likely also generated from the oxidation of later-generation products, such as catechol.

Because HBA had a much larger HBA and benzaldehyde both exhibit potential for high SOA yields. HBA may have a slightly higher SOA yield than benzaldehyde and a large branching ratio fraction from benzyl alcohol oxidation, HBA likely contributed most therefore HBA contributes significantly to the large measured SOA yield of benzyl alcohol in our experiments. We estimate, by competitive kinetics, that the reaction of HBA + OH proceeds at $(2 \pm 0.1) \times 10^{-11} \text{ cm}^3 \text{ molecule}^{-1} \text{ s}^{-1}$ (Appendix

305 ~~??). The rapid reaction of HBA likely leads to other products with increasing OH kinetics.~~ In aromatic oxidation chemistry, addition of electron-donating groups (such as OH) lowers the barrier of reaction for additional OH chemistry (Calvert et al., 2002). ~~With benzene~~In previously studied aromatic systems, adding electron-donating substituent groups can ~~increases~~increase reactivity with OH ~~by ~4–8x~~(Calvert et al., 2002). In the benzyl alcohol system, after every subsequent reaction with the OH radical, we anticipate the kinetics of HBA quickly lead to low-volatility, highly-oxygenated products that readily partition into aerosol. The rapid reaction of HBA leads catechol and other products that react quickly with OH.

310 ~~HBA predominately contributing to SOA further agrees with past SOA studies of benzyl alcohol conducted as a function of NO. In Charan et al. (2020), SOA yields of benzyl alcohol increased with decreasing NO. Similarly, here we observed that in gas-phase experiments (G1–3), the HBA yield increased with decreasing NO. Because HBA primarily contributed to the high SOA yield of benzyl alcohol, it follows that as the gas-phase yield of HBA increased, the SOA yield of benzyl alcohol also increased.~~

3.3 Comparison With Past Work

Past studies have detected HBA and benzaldehyde from the oxidation of benzyl alcohol (Wang, 2015; Bernard et al., 2013; Harrison and Wells, 2009). ~~Wang (2015) estimates the yield of~~We estimate the branching fraction to HBA of $(36 \pm 18)\%$. ~~In comparison, Wang (2015) calculated o-HBA is branching of~~11% using theoretical ~~estimates~~methods, while Bernard and 320 coworkers ~~estimate the yield is 21%~~; at similar NO we found the branching of HBA is $\sim 45\%$. We observed the HBA branching ratio increases with decreasing NO. In the absence of NO we found the yield is $\sim 69\%$. Variations in yields are likely due to differences in initial conditions. Though NO may have been similar across different works, yields are also affected by O₂, the initial benzyl alcohol mixing ratio, amount of benzyl alcohol reacted, OH exposure, and temperature, among other variables. In Bernard et al. (2013) starting benzyl alcohol mixing ratios ranged from ~ 2000 ppb–850 ppb, whereas in our system initial 325 benzyl alcohol < 100 ppb. If the system is allowed to react for sufficiently long, secondary chemistry can play an increasingly significant role. Unaccounted for secondary reactions may lead to an under-reporting of the HBA branching ratio, especially in longer oxidation experiments. Additionally, to our knowledge, no yield studies have been previously conducted for this system in the absence of NO. ~~estimated the branching fraction is 21%~~. The differences with Bernard et al. likely reflects the challenges of quantifying HBA and accounting for its very fast reactivity.

330 We observed only one isomer of HBA which we assume to be the *ortho* product. This assignment is based on past work that suggests the *ortho* position is a major product in aromatic oxidation chemistry by OH (Harrison and Wells, 2009; Finlayson-Pitts, Barbara and Pitts, James N. Jr., 1986; Baltaretu et al., 2009). Similarly, Wang (2015) predicted a single stable isomer of HBA, *ortho*. If additional HBA isomers existed in our system, it is likely they would have eluted at higher temperatures than were allowed by the current GC temperature profiles and were therefore undetected. However, secondary isomer formation is 335 typically considered to be minor in other aromatic systems (Finlayson-Pitts, Barbara and Pitts, James N. Jr., 1986; Baltaretu et al., 2009).

Bernard et al. (2013) also reported a benzaldehyde yield of ~~25%~~ $(25 \pm 4)\%$ (which was used as input to the computations performed in Wang 2015), while Harrison and Wells report a yield of 24% (no error provided) (Bernard et al., 2013; Wang,

2015; Harrison and Wells, 2009). We report a benzaldehyde ~~yield of ~19%~~^{averaged branching fraction of (21 ± 10)%}, in close
340 agreement with ~~past work. Closer agreement between our work and past work may be because benzaldehyde oxidation is not dependent on NO, unlike HBA, these studies.~~

4 Conclusions

Benzyl alcohol oxidizes via OH to primarily form HBA and benzaldehyde. Significant additional chemistry occurred via ~~endoeylization~~^{endo-cyclization} following addition of oxygen to fragmentation products such as ~~hydroxy oxpentalen~~^{5-hydroxy-4-oxo-2-pen}
345 and butadiene. We found that [NO] ~~has an effect on several of the product yields including HBA and hydroxy oxpentalen, though the overall relative distribution of oxidation products remained unchanged—namely that does not affect product yields for HBA, benzaldehyde, or 5-hydroxy-4-oxo-2-pentalen.~~ HBA was the dominant first-generation product with a branching ratio of ~~69–45%~~^{fraction of ~36%} over a range of NO conditions. The branching ~~ratio of benzaldehyde did not appear to be NO-dependent and fraction of benzaldehyde~~ is estimated to be ~~~19%~21%~~.

350 Both HBA and benzaldehyde ~~pathways~~ go on to form highly oxygenated gas-phase products. HBA oxidation leads to the formation of ~~products such as dihydroxybenzyl alcohol, while similarly, catechol and dihydroxybenzyl alcohol. Similarly,~~ benzaldehyde oxidation forms products such as dihydroxy benzoic acid. These products indicate that subsequent OH addition to the aromatic ring ~~occurred~~^{occur} in both pathways. Both the addition and ~~hydrogen~~ abstraction routes may ~~have~~ also contribute to the formation of C6 products.

355 Aerosol yield studies using HBA and benzaldehyde as the precursors suggested that the HBA pathway is ~~important a very important contributor~~ to the high SOA yields observed in benzyl alcohol oxidation. HBA is quickly oxidized by OH ~~($k_{OH} = (2 \pm 0.1) \times 10^{-11} \text{ cm}^3 \text{ molecule}^{-1} \text{ s}^{-1}$) to form to form~~^{catechol and subsequently to} low-volatility products which rapidly partition to the particle phase, thus contributing to the high SOA yield of benzyl alcohol. Though VCPs have been identified as increasingly important to SOA formation, key VOC components of VCPs remain uncharacterized. Products from benzyl
360 alcohol oxidation via OH were identified here, elucidating its fast reactivity and high aerosol mass yields.

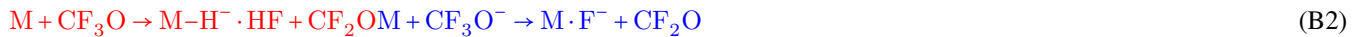
Data availability. Data from this study can be made available upon request. Data for experiments P1 and P2 can be found through the Integrated Chamber Atmospheric Data Repository for Unified Science (ICARUS) and upon request.

Appendix A: Experimental Conditions

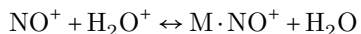
CH₃ONO (synthesized following Taylor et al. (1980)), and NO (1993±20 ppmv, Matheson) were injected into the Chamber G
365 (~ 800 L) in a similar fashion. The analyte is introduced to an evacuated 0.5 L glass bulb and is serially diluted with N₂ until the desired mixing ratio is achieved. CH₃ONO was quantified via FTIR spectroscopy using tabulated cross section prior to being injected into Chamber G. Ultraviolet lights (~~Sylvania~~^{8 bulbs Sylvania F40/350BL 40 W}) centered around 350 nm were used. The measured j_{CH_3ONO} and inferred j_{NO_2} from these lights are $1.1 \times 10^{-3} \text{ s}^{-1}$ and $4.4 \times 10^{-3} \text{ s}^{-1}$, respectively ~~for Chamber G~~.

Appendix B: CIMS Calibration and Instrument Sensitivity

370 The CIMS operates CF_3O^- ions are produced by flowing the reagent ion source (CF_3OOCF_3 in negative mode and $\text{NO}\cdot\text{H}_2\text{O}^+$ in positive mode) through a radioactive source (^{210}Po), generating the reagent ions. Similarly, $\text{NO}^+\cdot\text{H}_2\text{O}$ is formed by flowing NO . In negative mode, cluster ions CF_3O^- ions react with multifunctional organic compounds to form either clusters (Eq. B1) or F^- transfer ions (Eq. B2) are produced. CF_3O^- CIMS chemistry is documented extensively in past studies (Vasquez et al., 2018; St. Clair et al., 2010; Crounse et al., 2006). In short, the CF_3O^- ion is sensitive to a variety of atmospherically-relevant 375 oxygenated species.



380 In positive mode, $\text{NO}\cdot\text{H}_2\text{O}^+$ is produced $\text{NO}^+\cdot\text{H}_2\text{O}$ is used (Eq. B3). Ambient N_2 and H_2O react with NO . The $\text{NO}\cdot\text{H}_2\text{O}^+$ tends to bind to The $\text{NO}^+\cdot\text{H}_2\text{O}$ binds to less oxygenated species than CF_3O^- including carbonyls such as benzaldehyde.



385 The CIMS and GC-FID in experiments in Chamber P was were calibrated for benzyl alcohol and benzaldehyde, respectively. The GC-CIMS and GC-FID in experiments in Chamber G was were calibrated for phenol and benzaldehyde, respectively. Individual calibrants were injected into a ~100 L Teflon pillow bag using the same injection method as described previously. The sample was then measured via a Fourier transform infrared (FTIR) spectrometer with a path length of 19 cm. The reference FTIR spectrum from the Pacific Northwest National Laboratory (PNNL) database was used to tabulate cross sections to determine the exact concentration of the calibrant (Schwantes et al., 2017). The pillow bag was then diluted using dry N_2 and 390 sampled to determine the instrumental sensitivity. The GC-FID was calibrated using benzaldehyde and a similar procedure. In some cases, an averaged sensitivity was used for compounds as described in Xu et al. (2019).

Standards of catechol and D5-phenol were prepared from temperature-controlled permeation tubes which were weighed periodically to quantify their emission rates. These standards were then used to calibrate the GC-CIMS for these compounds. The measured and calculated catechol sensitivity (determined relative to phenol) agree within 28% of each other.

395 For hydroxy-oxopentenal, glycolaldehyde was used as a proxy, as detailed in Yu et al. Yu, Hongmin et al. (2023). In short, calculated dipole moments and polarizability of glycolaldehyde other less volatile analytes the calculated ion-molecule collision

Compound	Average Dipole (D) at 298 K	Polarizability (Å ³)
Phenol	1.828	10.07
Catechol	2.364	10.76
o-Hydroxy benzyl alcohol (o-HBA)	2.109	12.63
p-Hydroxy benzyl alcohol (p-HBA)	1.286	12.76
Benzyl alcohol	1.457	1.780
Z-5OH-4CO-pent-2-enal	3.072	10.55
E-5OH-4CO-pent-2-enal	2.015	10.80
o-Hydroxy benzaldehyde	3.008	12.64

Table B1. Quantum calculations of dipole moments and polarizabilities (at the B3LYP/cc-pVTZ level).

rate was used, relative to phenol (for G1 - G4) or benzyl alcohol (for P1), to estimate the CIMS sensitivities. The sensitivity of o-HBA, p-HBA, 5-hydroxy-4-oxo-2-pentenal, catechol, and benzyl alcohol (G1 - G4) were estimated in this way. Average

dipole moments at 298 K and polarizabilities (at B3LYP/cc-pVTZ level). These calculations are then used to determine the

400 compound-specific sensitivity to the CIMS signal. Glycolaldehyde was chosen as a proxy compound for hydroxy oxopentenal

because of their structural similarities and thus their similar chemistry with the reagent ion were calculated for all analytes

of interest (Table B1). These were used to calculate the ion-collision rate between analytes and reagent ion as described in ?

Assuming that the clusters are well bound, the sensitivity for a given analyte relative to a reference (here phenol) has been shown to be well represented by the ratio of their ion-molecule collision rates (Murphy et al., 2023).

405 For hydroxybenzyl alcohol (HBA), catechol was used as a calibrant proxy relative to phenol. Catechol was selected as a

proxy for HBA because of their similarities in structure, namely the two hydroxyl groups. Based on this functionalization, both HBA and catechol primarily bind with the transfer ion, F⁻.

Benzyl alcohol and phenol were calibrated directly For particle-phase experiments, HBA was calibrated on the CIMS for

particle-phase experiments using the method describe in the Calibration section of the main paper. These calibrations were

410 then used to estimate the relative to the CIMS sensitivity of benzyl alcohol for the by comparing the relative GC-CIMS used

sensitivities of HBA and benzyl alcohol in gas-phase experiments. These calculations were performed based on the assumption that the same yield of phenol will form from benzyl alcohol under similar conditions (e.g., initial NO).

Catechol and phenol were calibrated using permeation tubes which were weighed to determine the exact mass of analyte.

This known amount substrate was then correlated to signal on the GC-CIMS.

415 Appendix C: GC Operation

In gas-phase experiments, analyte samples were cryogenically trapped in the GC-CIMS for 10 mins on the head of the 20

m, Restek RTX1701 at ~ -20°C for 10 mins using liquid CO₂. The sample was then eluted through the GC using a ramp of

10°C/min to 55°C and then 2.5°C/min to 130°C. The slower ramp rate from 55 – 130°C was used because most oxidation

products eluted at this time and using a slower ramp ensured relevant products were sufficiently separated. When GC scans

420 were not being taken, the CIMS sampled directly from the reaction chamber. For

For the particle-phase experiments, the GC-FID was run from 40°C to 250° C with a ramp rate of 50°C/min. For gas-phase experiments, however, where benzyl alcohol was used as the precursor, we were interested in detecting and quantifying both benzaldehyde and benzyl alcohol. A DB-5 column was used for these experiments. column in the GC-FID was used for all experiments.

425 **Appendix D: The Reaction Rate Coefficient for OH + HBA**

Relative rate of reaction of HBA compared to butanediol.

Relative rate experiments of HBA were conducted using butanediol as a reference. The assumed kinetic rate constant for butanediol was $(2.7 \pm 0.48) \times 10^{-11} \text{ cm}^3 \text{ molecule}^{-1} \text{ s}^{-1}$ Bethel et al. (2001). Methods to calculate k_{OH} are detailed in Bethel et al. (2001) Bethel et al. (2001). In brief, ~20 ppb of 1,2-butanediol was injected into Chamber G using the procedure described in Methods. Similar amounts of HBA were also injected. Methyl nitrate (~500 ppb) was used as the oxidant source and ~333 ppb of NO (Matheson, 1993 ± 20 ppb) was also injected. Oxidation was initiated using 8 UV lights (Sylvania) centered around 350 nm lights. Short periods of oxidation (~1 min) were followed by periods without irradiation to allow the CIMS signal to stabilize. This proceeded until approximately one e-fold of VOC was reacted. The plotted natural log quotients of initial and final mixing ratios of butanediol and HBA can be found in Figure ???. The slope of this plot provides a ratio of their respective kinetic rate constants:

$$\text{slope} = \frac{k_{\text{HBA}}}{k_{\text{diol}}}$$

The slope of the natural log quotients can be found in Figure ???. Based on these data, the relative rate of HBA is $(2 \pm 0.1) \times 10^{-11} \text{ cm}^3 \text{ molecule}^{-1} \text{ s}^{-1}$

440 **Appendix D: Parameterization of SOA Yields**

We report the results of the parameters from the least square fit for benzaldehyde derived SOA. For Eq. 6, $\alpha = 0.34 \pm 0.013$ and $K_{\text{om}} = (9.4 \pm 1.2) \times 10^{-3}$. The fit has an r-squared value of 0.90.

445 **Appendix D: Oxidation Products Detected**

The following table summarizes masses detected by the GC-CIMS in gas-phase experiments (G1 - G3). While some products were identified using authentic standards, other assignments are based on masses detected and our chemical understanding of this and other aromatic systems.

VOC Compound (m/z)	Structure	Formula	Observed m/z and Reagent Ion
Benzyl alcohol (108)		$C_6H_5CH_2OH$	193 (CF_3O^-)
Benzaldehyde (106)		$C_6H_5C(O)$	136 (NO^+)
Hydroxybenzyl alcohol (124)		$C_6H_4OHCH_2OH$	143 (F^-) and 209 (CF_3O^-)
Dihydroxybenzyl alcohol (140)		$C_6H_4OHOHCH_2OH$	225 (CF_3O^-)
Phenol (94)		C_6H_5OH	113 (F^-) and 179 (CF_3O^-)
Catechol (110)		C_6H_4OHOH	129 (F^-) and 195 (CF_3O^-)
Nitrophenol (139)		$C_6H_5NO_3$	158 (F^-)
Dihydroxybenzoic acid (154)		$C_6H_3OHOHC(O)OH$	173 (F^-)
Tetrahydroxy benzene (142)		$C_6H_6O_4$	161 (F^-)
Glyoxal (58)		$C_2H_2O_2$	88 (NO^+)
Butenedial (84)		$C_4H_4O_2$	114 (NO^+)
Oxopropanoic acid (88)		$C_3H_4O_3$	173 (CF_3O^-)
5-hydroxy-4-oxo-2-pentenal (114)		$C_5O_3H_6$	199 (CF_3O^-)
Hydroxyacetaldehyde (60)		$C_2O_2H_4$	145 (CF_3O^-)

Table D1. Compound assignments from CIMS data. Note that several of the compounds listed have many isomeric structures though only one may be listed as an example.

Appendix E: Estimation of Uncertainty

In gas phase experiments, the major source of error in our calculation of ~~yields branching ratios~~ comes from the ~~relative sensitivity of the product concentration as measured by their respective instruments~~ knowledge of the CIMS sensitivity to the analytes measured. A part of the ~~uncertainty~~ comes from propagating the error of phenol calibrated via the permeation tubes since several of the analytes were calibrated relative to phenol. Some uncertainty is also derived from the calculated ion-molecule collision rates which were based on the computationally derived dipole moments and polarizabilities. A smaller part of the ~~reported~~ error is also determined ~~by calculating from~~ the standard deviation of ~~signal variations~~ signals. This varies from compound to compound and is also dependent on the reagent gas used. ~~Uncertainty in quantifying the relative signals in positive and negative. As an example, catechol was calibrated both using the permutation tube method and using the computational method. The two calibration factors varied by ~ 28%. Based on this, we estimate the error for compounds detected by the GC-CIMS is ~ 63%. Phenol was directly calibrated for branching ratio calculations, therefore the estimated uncertainty for phenol is 21% the normalized branching fractions to be ~ 45%, congruent with past work using similar experimental setups (Praske et al., 2018; ?). HBA branching ratios have a slightly higher uncertainty because of our treatment of its secondary chemistry (see Section 2.3.2).~~

460 Appendix F: OH Exposure

[OH] was calculated for SOA yield experiments using the kinetic equation:

$$\frac{d[\text{reagent}]}{dt} = -k_{\text{OH}}[\text{OH}][\text{reagent}] \quad (\text{F1})$$

Here, $\frac{d[\text{reagent}]}{dt}$ was determined by finding the ~~log of the~~ slope of the starting reagent against time. For benzaldehyde, the ~~log of the~~ slope over the entire experiment was used ~~and assuming~~ $k_{\text{OH}} = (1.29 \pm 0.32) \times 10^{-11} \text{ cm}^3 \text{ molec}^{-1} \text{ s}^{-1}$. For HBA, the ~~log of the~~ slope for the first 15 min was used to determine [OH] for the experiment, ~~and assuming~~ k_{OH} of HBA = $(5.59 \pm 2.2) \times 10^{-11} \text{ cm}^3 \text{ molec}^{-1} \text{ s}^{-1}$.

Appendix G: Wall-Loss

Particle wall loss was accounted for in SOA yield experiments using methods described in Charan et al. (2020) and Charan et al. (2018). In short, the SOA data were fit by parameterizing the eddy diffusivity coefficient (k_e). The mean electric field experienced within the chamber (E) was assumed to be zero because the environmental chambers are enclosed and undisturbed prior to the experiments and therefore have no charge source. For experiment P1, $k_e = 0.720$ was used and for experiment P2, $k_e = 0.346$ was used.

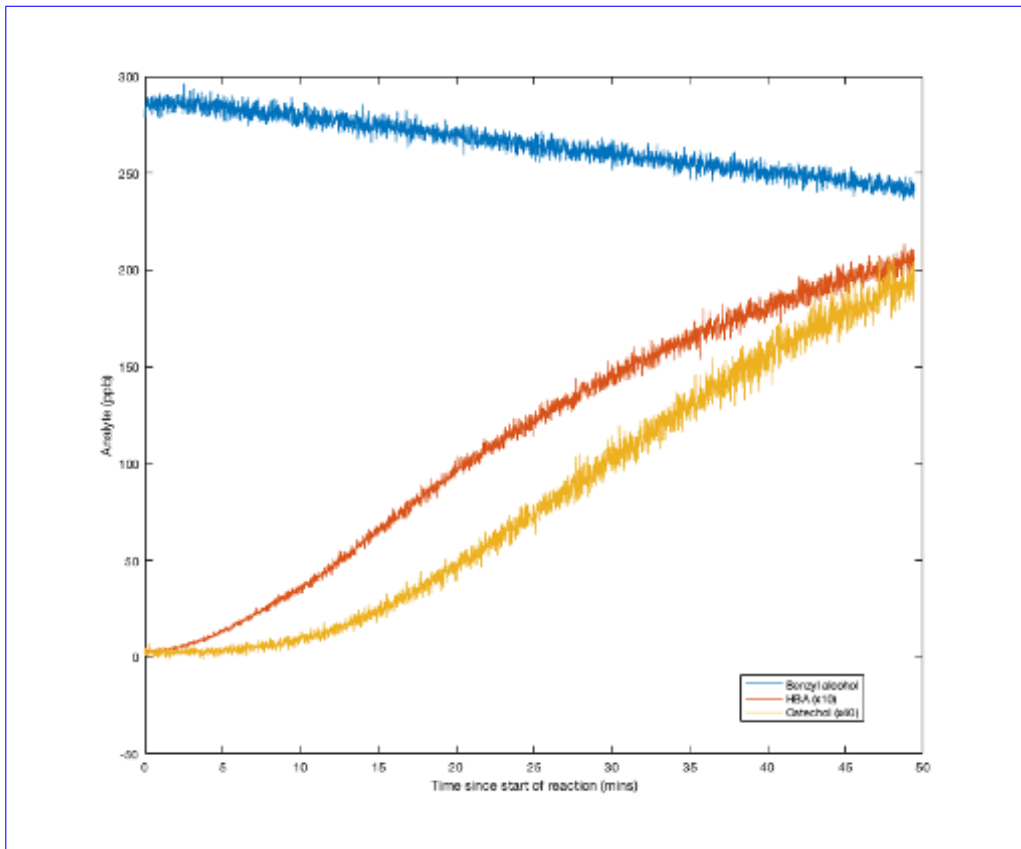


Figure H1. Consistent with a previous study (cite), catechol is a major oxidation product of hydroxybenzyl alcohol (HBA). Note that the compounds are displayed here as x10 (HBA) and x40 (catechol).

Appendix H: Secondary Chemistry

We use the kinetics of cresol to estimate $k_{\text{OH}+\text{HBA}}$ in order to make secondary chemistry corrections for the branching ratio of HBA. $K_{\text{OH}+\text{cresol}}$ is used because of its similar structure to HBA. We use a structure additivity correction to account for the abstractable hydrogens of HBA compared to cresol. We find that this rate is broadly consistent with the observed time dependence of HBA and catechol (Figure H1).

Appendix I: Excluded Data

One experiment was excluded from the data presented. This gas-phase experiment was run under similar conditions to those reported in the main text and with 0 ppb NO. This experiment was excluded because the relatively low amount of benzyl alcohol reacted resulted in very large uncertainty in the branching fractions of HBA and benzaldehyde.

Author contributions. RSB: study conceptualization, data collection and analysis, result interpretation, and writing. SMC: Analysis code and writing. JHS: supervision and writing. POW: supervision, result interpretation, and writing.

Competing interests. The authors have no competing interests to declare.

485 *Acknowledgements.* This research was supported by the National Science Foundation (grant no. CHE-2305204) and the Alfred P. Sloan Foundation (grant no. G-2019-12281). Work performed by RSB was supported by the National Science Foundation Graduate Research Fellowship (grant no. 1745301). The authors thank Yuanlong Huang for help troubleshooting instrumentation in the lab~~and Lu-Xu and Katharine Ball for their work on phenol and catechol calibrations~~, Nathan Dalleska for his insights on the GC-FID, and Katherine Ball for calibrations. We thank Prof. Henrik Kjaeragard, Copenhagen University, for providing the dipole moments and polarizabilities listed in Table 490 B1.

References

Atkinson, R., Aschmann, S. M., Carter, W. P. L., Wlner, A. M., and Pitts, J. N.: Alkyl Nitrate Formation from the NO_x-Air Photooxidations of C2-C8 n-Alkanes, *Journal of Physical Chemistry, The*, 86:23, 7, <https://doi.org/10.1021/j100220a022>, 1982.

Baltaretu, C. O., Lichtman, E. I., Hadler, A. B., and Elrod, M. J.: Primary Atmospheric Oxidation Mechanism for Toluene, *The Journal of Physical Chemistry A*, 113, 221–230, <https://doi.org/10.1021/jp806841t>, 2009.

495 Bernard, F., Magneron, I., Eyglunent, G., Daële, V., Wallington, T. J., Hurley, M. D., and Mellouki, A.: Atmospheric Chemistry of Benzyl Alcohol: Kinetics and Mechanism of Reaction with OH Radicals, *Environmental Science & Technology*, 47, 3182–3189, <https://doi.org/10.1021/es304600z>, 2013.

Bethel, H. L., Atkinson, R., and Arey, J.: Kinetics and products of the reactions of selected diols with the OH radical, *International Journal 500 of Chemical Kinetics*, 33, 310–316, <https://doi.org/10.1002/kin.1025>, 2001.

Birdsall, A. W., Andreoni, J. F., and Elrod, M. J.: Investigation of the Role of Bicyclic Peroxy Radicals in the Oxidation Mechanism of Toluene, *The Journal of Physical Chemistry A*, 114, 10 655–10 663, <https://doi.org/10.1021/jp105467e>, 2010.

Bloss, C., Wagner, V., Jenkin, M. E., Volkamer, R., Bloss, W. J., Lee, J. D., Heard, D. E., Wirtz, K., Martin-Reviejo, M., Rea, G., Wenger, J. C., and Pilling, M. J.: Development of a detailed chemical mechanism (MCMv3.1) for the atmospheric oxidation of aromatic hydrocarbons, 505 *Atmos. Chem. Phys.*, 2005.

Burkholder, J. B., Abbatt, J. P. D., Barnes, I., Roberts, J. M., Melamed, M. L., Ammann, M., Bertram, A. K., Cappa, C. D., Carlton, A. G., Carpenter, L. J., Crowley, J. N., Dubowski, Y., George, C., Heard, D. E., Herrmann, H., Keutsch, F. N., Kroll, J. H., McNeill, V. F., Ng, N. L., Nizkorodov, S. A., Orlando, J. J., Percival, C. J., Picquet-Varrault, B., Rudich, Y., Seakins, P. W., Surratt, J. D., Tanimoto, H., Thornton, J. A., Tong, Z., Tyndall, G. S., Wahner, A., Weschler, C. J., Wilson, K. R., and Ziemann, P. J.: The Essential Role for Laboratory 510 Studies in Atmospheric Chemistry, *Environmental Science & Technology*, 51, 2519–2528, <https://doi.org/10.1021/acs.est.6b04947>, 2017.

Calvert, J. G., Atkinson, Roger, Becker, Karl H., Kamens, Richard M., Seinfeld, J. H., Wallington, Timothy J., and Yarwood, Greg: Mechanism of Atmospheric Oxidation of Aromatic Hydrocarbons, The, Oxford University Press, New York, New York, 2002.

Chan, M. N., Surratt, J. D., Claeys, M., Edgerton, E. S., Tanner, R. L., Shaw, S. L., Zheng, M., Knipping, E. M., Eddingsaas, N. C., Wennberg, P. O., and Seinfeld, J. H.: Characterization and Quantification of Isoprene-Derived Epoxydiols in Ambient Aerosol in the Southeastern 515 United States, *Environmental Science & Technology*, 44, 4590–4596, <https://doi.org/10.1021/es100596b>, 2010.

Charan, S. M., Kong, W., Flagan, R. C., and Seinfeld, J. H.: Effect of particle charge on aerosol dynamics in Teflon environmental chambers, *Aerosol Science and Technology*, 52, 854–871, <https://doi.org/10.1080/02786826.2018.1474167>, 2018.

Charan, S. M., Buenconsejo, R. S., and Seinfeld, J. H.: Secondary organic aerosol yields from the oxidation of benzyl alcohol, *Atmospheric Chemistry and Physics*, 20, 13 167–13 190, <https://doi.org/10.5194/acp-20-13167-2020>, 2020.

520 Charan, S. M., Huang, Y., Buenconsejo, R. S., Li, Q., Cocker III, D. R., and Seinfeld, J. H.: Secondary organic aerosol formation from the oxidation of decamethylcyclopentasiloxane at atmospherically relevant OH concentrations, *Atmospheric Chemistry and Physics*, 22, 917–928, <https://doi.org/10.5194/acp-22-917-2022>, 2022.

Coggon, M. M., Gkatzelis, G. I., McDonald, B. C., Gilman, J. B., Schwantes, R. H., Abuhassan, N., Aikin, K. C., Arend, M. F., Berkoff, T. A., Brown, S. S., Campos, T. L., Dickerson, R. R., Gronoff, G., Hurley, J. F., Isaacman-VanWertz, G., Koss, A. R., Li, M., Mc-525 Keen, S. A., Moshary, F., Peischl, J., Pospisilova, V., Ren, X., Wilson, A., Wu, Y., Trainer, M., and Warneke, C.: Volatile chemical product emissions enhance ozone and modulate urban chemistry, *Proceedings of the National Academy of Sciences*, 118, e2026653 118, <https://doi.org/10.1073/pnas.2026653118>, 2021.

Crounse, J. D., McKinney, K. A., Kwan, A. J., and Wennberg, P. O.: Measurement of Gas-Phase Hydroperoxides by Chemical Ionization Mass Spectrometry, *Analytical Chemistry*, 78, 6726–6732, <https://doi.org/10.1021/ac0604235>, 2006.

530 Finlayson-Pitts, Barbara and Pitts, James N. Jr.: *Atmospheric Chemistry: Fundamentals and Experimental Techniques*, Wiley-Interscience, United States, 1986.

Griffith, S. M., Hansen, R. F., Dusanter, S., Michoud, V., Gilman, J. B., Kuster, W. C., Veres, P. R., Graus, M., Gouw, J. A., Roberts, J., Young, C., Washenfelder, R., Brown, S. S., Thalman, R., Waxman, E., Volkamer, R., Tsai, C., Stutz, J., Flynn, J. H., Grossberg, N., Lefer, B., Alvarez, S. L., Rappenglueck, B., Mielke, L. H., Osthoff, H. D., and Stevens, P. S.: Measurements of hydroxyl and hydroperoxy radicals during CalNex-LA: Model comparisons and radical budgets, *Journal of Geophysical Research: Atmospheres*, 121, 4211–4232, <https://doi.org/10.1002/2015JD024358>, 2016.

535 Harrison, J. C. and Wells, J.: Gas-phase chemistry of benzyl alcohol: Reaction rate constants and products with OH radical and ozone, *Atmospheric Environment*, 43, 798–804, <https://doi.org/10.1016/j.atmosenv.2008.11.001>, 2009.

Huang, Y., Zhao, R., Charan, S. M., Kenseth, C. M., Zhang, X., and Seinfeld, J. H.: Unified Theory of Vapor-Wall Mass Transport in 540 Teflon-Walled Environmental Chambers, *Environmental Science & Technology*, 52, 2134–2142, <https://doi.org/10.1021/acs.est.7b05575>, 2018.

Jaoui, M., Docherty, K. S., Lewandowski, M., and Kleindienst, T. E.: Yields and molecular composition of gas-phase and secondary organic aerosol from the photooxidation of the volatile consumer product benzyl alcohol: formation of highly oxygenated and hydroxy nitro-aromatic compounds, *Atmospheric Chemistry and Physics*, 23, 4637–4661, <https://doi.org/10.5194/acp-23-4637-2023>, 2023.

545 Jenkin, M. E., Saunders, S. M., Wagner, V., and Pilling, M. J.: Protocol for the development of the Master Chemical Mechanism, MCM v3 (Part B): tropospheric degradation of aromatic volatile organic compounds, Part B, 2003.

Li, L. and Cocker, D. R.: Molecular structure impacts on secondary organic aerosol formation from glycol ethers, *Atmospheric Environment*, 180, 206–215, <https://doi.org/10.1016/j.atmosenv.2017.12.025>, 2018.

Mai, H.: Scanning Electrical Mobility Methods for Aerosol Characterization, Ph.D. thesis, California Institute of Technology, 10.7907/ 550 9D4H-QS44, 2018.

Martín, P., Cabañas, B., Colmenar, I., Salgado, M. S., Villanueva, F., and Tapia, A.: Reactivity of E-butenedial with the major atmospheric oxidants, *Atmospheric Environment*, 70, 351–360, <https://doi.org/10.1016/j.atmosenv.2013.01.041>, 2013.

McDonald, B. C., de Gouw, J. A., Gilman, J. B., Jathar, S. H., Akherati, A., Cappa, C. D., Jimenez, J. L., Lee-Taylor, J., Hayes, P. L., 555 McKeen, S. A., Cui, Y. Y., Kim, S.-W., Gentner, D. R., Isaacman-VanWertz, G., Goldstein, A. H., Harley, R. A., Frost, G. J., Roberts, J. M., Ryerson, T. B., and Trainer, M.: Volatile chemical products emerging as largest petrochemical source of urban organic emissions, *Science*, 359, 760–764, <https://doi.org/10.1126/science.aaq0524>, 2018.

Murphy, S. E., Crounse, J. D., Møller, K. H., Rezgui, S. P., Hafeman, N. J., Park, J., Kjaergaard, H. G., Stoltz, B. M., and Wennberg, P. O.: Accretion product formation in the self-reaction of ethene-derived hydroxy peroxy radicals, *Environmental Science: Atmospheres*, 3, 882–893, <https://doi.org/10.1039/D3EA00020F>, 2023.

560 Namysl, S., Pelucchi, M., Pratali Maffei, L., Herbinet, O., Stagni, A., Faravelli, T., and Battin-Leclerc, F.: Experimental and modeling study of benzaldehyde oxidation, *Combustion and Flame*, 211, 124–132, <https://doi.org/10.1016/j.combustflame.2019.09.024>, 2020.

Odum, J. R., Hoffmann, T., Bowman, F., Collins, D., Flagan, R. C., and Seinfeld, J. H.: Gas/Particle Partitioning and Secondary Organic Aerosol Yields, *Environmental Science & Technology*, 30, 2580–2585, <https://doi.org/10.1021/es950943+>, 1996.

Parker, H. A., Hasheminassab, S., Crounse, J. D., Roehl, C. M., and Wennberg, P. O.: Impacts of Traffic Reductions Associated With 565 COVID-19 on Southern California Air Quality, *Geophysical Research Letters*, 47, <https://doi.org/10.1029/2020GL090164>, 2020.

Paulot, F., Crounse, J. D., Kjaergaard, H. G., Kürten, A., St. Clair, J. M., Seinfeld, J. H., and Wennberg, P. O.: Unexpected Epoxide Formation in the Gas-Phase Photooxidation of Isoprene, *Science*, 325, 730–733, <https://doi.org/10.1126/science.1172910>, 2009.

Pennington, E. A., Seltzer, K. M., Murphy, B. N., Qin, M., Seinfeld, J. H., and Pye, H. O. T.: Modeling secondary organic aerosol formation from volatile chemical products, *Atmospheric Chemistry and Physics*, 21, 18 247–18 261, <https://doi.org/10.5194/acp-21-18247-2021>, 570 2021.

Praske, E., Otkjær, R. V., Crounse, J. D., Hethcox, J. C., Stoltz, B. M., Kjaergaard, H. G., and Wennberg, P. O.: Atmospheric autoxidation is increasingly important in urban and suburban North America, *Proceedings of the National Academy of Sciences*, 115, 64–69, 575 <https://doi.org/10.1073/pnas.1715540115>, 2018.

Rinke, M. and Zetzsch, C.: Rate Constants for the Reactions of OH Radicals with Aromatics: Benzene, Phenol, Aniline, and 1,2,4-Trichlorobenzene, *Berichte der Bunsengesellschaft für physikalische Chemie*, 88, 55–62, <https://doi.org/10.1002/bbpc.19840880114>, 1984.

Schwantes, R. H., Schilling, K. A., McVay, R. C., Lignell, H., Coggon, M. M., Zhang, X., Wennberg, P. O., and Seinfeld, J. H.: Formation of highly oxygenated low-volatility products from cresol oxidation, *Atmospheric Chemistry and Physics*, 17, 3453–3474, 580 <https://doi.org/10.5194/acp-17-3453-2017>, 2017.

Seinfeld, J. H. and Pandis, S. N.: *Atmospheric chemistry and physics: from air pollution to climate change*, John Wiley & Sons, Hoboken, New Jersey, third edition edn., 2016.

Seltzer, K. M., Pennington, E., Rao, V., Murphy, B. N., Strum, M., Isaacs, K. K., and Pye, H. O. T.: Reactive organic carbon emissions from volatile chemical products, *Atmospheric Chemistry and Physics*, 21, 5079–5100, <https://doi.org/10.5194/acp-21-5079-2021>, 2021.

St. Clair, J. M., McCabe, D. C., Crounse, J. D., Steiner, U., and Wennberg, P. O.: Chemical ionization tandem mass spectrometer for the *in situ* measurement of methyl hydrogen peroxide, *Review of Scientific Instruments*, 81, 094 102, <https://doi.org/10.1063/1.3480552>, 585 2010.

Taylor, W., Allston, T., Moscato, M., Fazekas, G., Kozlowski, R., and Takacs, G.: Atmospheric photodissociation lifetimes for nitromethane, methyl nitrite, and methyl nitrate, *International Journal of Chemical Kinetics*, 12, 231–240, <https://doi.org/10.1002/kin.550120404>, 1980.

Vasquez, K. T., Allen, H. M., Crounse, J. D., Praske, E., Xu, L., Noelscher, A. C., and Wennberg, P. O.: Low-pressure gas chromatography with chemical ionization mass spectrometry for quantification of multifunctional organic compounds in the atmosphere, *Atmospheric Measurement Techniques*, 11, 6815–6832, <https://doi.org/10.5194/amt-2018-223>, 590 2018.

Wang, L.: The Atmospheric Oxidation Mechanism of Benzyl Alcohol Initiated by OH Radicals: The Addition Channels, *ChemPhysChem*, 16, 1542–1550, <https://doi.org/10.1002/cphc.201500012>, 2015.

Weitkamp, E. A., Sage, A. M., Pierce, J. R., Donahue, N. M., and Robinson, A. L.: Organic Aerosol Formation from Photochemical Oxidation of Diesel Exhaust in a Smog Chamber, *Environmental Science & Technology*, 41, 6969–6975, <https://doi.org/10.1021/es070193r>, 2007.

Xu, L., Møller, K. H., Crounse, J. D., Otkjær, R. V., Kjaergaard, H. G., and Wennberg, P. O.: Unimolecular Reactions of Peroxy Radicals Formed in the Oxidation of α -Pinene and β -Pinene by Hydroxyl Radicals, *The Journal of Physical Chemistry A*, 123, 1661–1674, 595 <https://doi.org/10.1021/acs.jpca.8b11726>, 2019.

Xu, L., Møller, K. H., Crounse, J. D., Kjaergaard, H. G., and Wennberg, P. O.: New Insights into the Radical Chemistry and Product Distribution in the OH-Initiated Oxidation of Benzene, *Environmental Science & Technology*, 54, 13 467–13 477, 600 <https://doi.org/10.1021/acs.est.0c04780>, 2020.

Yu, Hongmin, Moller, Kristian H., Buенконсеjo, Reina, Crounse, John, Kjaergaard, Henrik Grum, and Wennberg, Paul: Atmospheric photo-oxidation of 2-ethoxyethanol: autoxidation chemistry of glycol ethers, *Journal of Physical Chemistry, The, In Review*, 2023.

Zafonte, L., Rieger, P. L., and Holmes, J. R.: Nitrogen dioxide photolysis in the Los Angeles atmosphere, *Environmental Science & Technology*, 11, 483–487, <https://doi.org/10.1021/es60128a006>, 1977.